

Alternated Quinoid/Aromatic Units in Terthiophenes Building Blocks for Electroactive Narrow Band Gap Polymers. Extended Spectroscopic, Solid State, Electrochemical, and Theoretical Study

Juan Casado, Rocío Ponce Ortiz, Mari Carmen Ruiz Delgado, Víctor Hernández, and Juan T. López Navarrete*

Departamento de Química Física, Facultad de Ciencias, Universidad de Málaga, 29071 Málaga, Spain

Jean-Manuel Raimundo, Philippe Blanchard, Magali Allain, and Jean Roncali*

Groupe Systèmes Conjugués Linéaires, CIMMA UMR CNRS 6200, Université d'Angers, 2 Bd Lavoisier, 49045 Angers Cedex, France

Received: April 19, 2005; In Final Form: July 7, 2005

We report here the synthesis of three novel π -conjugated heterocyclic mixed trimers that contain two electron-donating 3,4-ethylenedioxy-2-thienyl (EDOT) units covalently attached to a central proquinoid electron-accepting thienopyrazine moiety (two of these narrow-HOMO–LUMO gap **D–A–D** compounds also bear hexyl side chains attached either to the outermost α positions of the EDOT end rings or to the β positions of the pyrazine fused ring). The modification of the terthiophene structure upon EDO, pyrazine, and hexyl substitutions has been treated in detail with spectroscopic and theoretical arguments. Solid-state properties reveal the occurrence of short intramolecular contacts between heteroatoms of adjacent rings. The analysis of the structure of the π -conjugated backbone of each molecule is consistent with a partial quinoid-like pattern which partially reverts to be subtly more aromatic depending on the topology of the positive inductive effect of the hexyl chains. This quinoidization is a consequence of the appearance of a **D**(EDOT)→**A**(PyT)←**D**(EDOT) intramolecular charge transfer which further polarizes the structure. The same chemical concepts have been applied to address their electrochemical behavior. The three mixed trimers exhibit amphoteric properties due to the combination of electron acceptor and donor groups. Given their relative low HOMO–LUMO energy gap, these trimers promise to be good candidates for obtaining polymers with significant low energy gap combining electroactivity.

I. Introduction

Much attention has been devoted over the past few years to the development of narrow-band gap π -conjugated polymers (i.e., $E_g < 1$ eV), which should behave among other technologically relevant physical properties as intrinsic electrical conductors.^{1,2} The synthetic principles for lowering the band gap have been reviewed.³ A reduction of the band gap of conjugated polymers can be accomplished, among other ways, by minimizing the bond length alternation (BLA) and by reducing the energy difference between aromatic and quinoid canonical structures such as in the case of polyisothianaphthene and soluble derivatives.⁴ One successful strategy to achieve narrow-band gap π -conjugated systems is based on the pioneering work by Havinga and co-workers^{5,6} and involves the alternation of electron-rich (donor, D) and electron-deficient (acceptor, A) units along the same conjugated chain. Many reports have described the electrochemical preparation of narrow-band gap polymers consisting of an alternating sequence of an electron-releasing bithiophene or *N,N'*-dimethylbipyrrole group and an electron-withdrawing moiety such as thieno[3,4-*b*]pyrazine, 2,1,3-benzothiadiazole, benzo[1,2-*c*:4,5-*c'*]bis[1,2,5]thiadiazole, or [1,2,5]thiadiazolo[3,4-*g*]quinoxaline. These poly(D–A) systems exhibit optical band gaps as low as 0.5 eV.^{2,7,8}

More recently, it has been shown that the association of 3,4-ethylenedioxythiophene (EDOT) as electron donating system with some of the above cited proquinoid acceptor groups could lead to polymers with a band gap among the lowest known to date (0.36 eV).^{9a,b} Furthermore, it has been also demonstrated that tricyclic systems based on such a combination could associate high fluorescence quantum yield, enhanced electron-affinity, and tunable absorption and emission spectra.^{9c}

These principles also apply to the design of the basic monomeric conjugated subunits. In particular, π -conjugated co-oligomers with alternating **-(D–A)-** structures and combining aromatic-donor and *o*-quinoid acceptor heterocycles are highly polarized and should display an intrinsically small HOMO–LUMO gap, thus leading to quite relevant properties for technological applications such as absorption in the near-infrared region, nonlinear optical properties, amphoteric redox behavior, and single component electrical conductivity.^{2,10} These π -extended systems have reduced on-site Coulomb repulsions, which are among the important requirements for the design of interesting new organic molecular materials. Highly polarized co-oligomers have also low excitation energies, and interesting optical properties such as nonlinear optical responses could be expected. On the other hand, it is of great benefit to combine electron-donating and accepting abilities; thus, when the various constituting heterocycles are properly balanced through the participation of the conjugated path, these compounds can show

* To whom correspondence should be addressed.

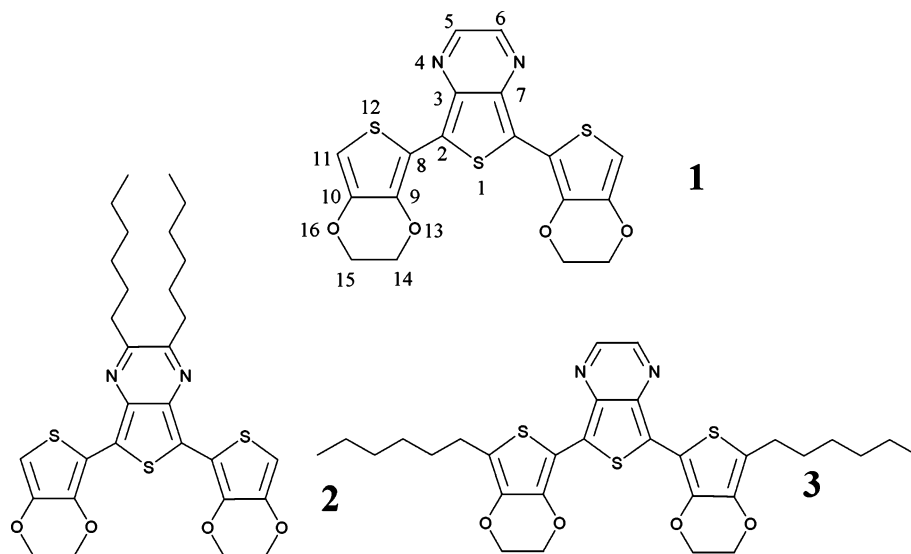


Figure 1. Chemical structures of the compounds and abbreviate notation to be used throughout the text (atom numbering is to be used for Table 4).

stable and relatively low energetic oxidations and reductions (amphoteric properties) which is of great interest to obtain ambipolar electroactivity.

Vis-NIR electronic absorption and infrared and Raman spectroscopies have been used from the discovery of the electrically conducting polymers to characterize many different classes of π -conjugated oligomers and polymers, and among them, Raman spectroscopy has been shown to be of great help in (i) estimating the degree of π -conjugation in neutral state,^{11–13} (ii) characterizing different types of conjugational defects in doped materials,¹⁴ and (iii) analyzing the efficiency of the intramolecular charge transfer in push–pull π -conjugated systems.¹⁵ The appearance of only a few and overwhelmingly strong Raman bands, even for systems with complex chemical structures, is a direct consequence, on the basis of the effective conjugation coordinate (ECC) theory,¹⁶ of the existence of a rather effective electron–phonon coupling over the whole quasi-one-dimensional π -conjugated backbone. In aromatic and heteroaromatic polyconjugated systems, the so-called as collective ECC vibrational coordinate (linear and collective combination of ring C=C/C–C stretchings spreading over the whole conjugated path) is at the origin of all of the measured Raman bands of the spectra in solid state. ECC theory states that upon increasing conjugation (more quinoid) length, the intense Raman bands undergo sizable dispersions toward lower wavenumber, whereas increasing the aromaticity of the whole path results in an opposite behavior of these Raman lines. Thus, changes in the peak positions and intensities of the Raman features upon terminal or side chain substitution are particularly useful in evaluating the aromatic \leftrightarrow quinoid participation in the description of the ground electronic state of a given series of neutral conjugated molecules with defined linear C=C/C–C path.

As part of the continuing interest of some of us in band gap engineering,⁹ here we report on the synthesis of three new tricyclic π -conjugated systems made up of a thienopyrazine unit with its two α -positions capped by electron-donating 3,4-ethylenedioxy-2-thienyl rings (i.e., two of these D–A–D compounds also bear hexyl side chains attached either to the outermost α positions of the EDOT end rings or to the β positions of the fused pyrazine ring). The electron-deficient central moiety is expected to have a strong propensity to impose a quinoid-like pattern on the ground-state structure of the three π -conjugated mixed trimers, thus leading to small intrinsic

HOMO–LUMO gaps. This work extends that previously done by some of us which dealt with tricyclic co-oligomers built up of proquinoid acceptors as benzo[*c*]thiophene or benzo[*c*]thiadiazole.^{9b} The insertion of these groups in short chain conjugated oligomers leads the control of their fluorescence efficiency and electron affinity. In this regard, our tricyclic molecules are the first of these series which are designed to precisely tune their NLO properties and amphoteric features which are determined by the suitable interplay in the ground electronic state of aromatic and quinoid contributions.

Thus, the interest of this work is focused on the optical absorptions, on the electrochemical activity, and on the vibrational features of these materials as determined by the existence of an aromatic/quinoid competition in the description of their electronic structure which, at the same time, will allow us to assess useful information about their π -conjugational properties and the degree of intramolecular charge transfer from the donor to the acceptor units. In addition, density functional theory (DFT) calculations are performed as a guide for the analysis of the spectroscopic features and to derive relevant molecular parameters.

II. Results and Discussion

A. Synthesis and UV–Vis Absorption Data. The chemical structures and notation of the three low-HOMO–LUMO gap mixed trimers studied in this paper are depicted in Figure 1. Compounds **1**–**3** were prepared, according to the synthetic procedure described in Scheme 1, through a Stille coupling of the corresponding 5,7-dibromothiopheno[3,4-*b*]pyrazine (**5a** or **5b**) with the tributylstannyl derivatives of EDOT (**9**) and 2-hexyl EDOT (**10**). Compounds **5a** and **5b** were obtained after a bromination of the corresponding thieno[3,4-*b*]pyrazines **4** in the presence of *N*-bromosuccinimide.^{17a} Compounds **9** and **10** were prepared respectively from EDOT (**6**) and 2-hexyleDOT (**8**) as described in the literature.^{17b,c} The synthesis of **8** was carried out in two successive steps starting from EDOT: (i) a Friedel–Craft acylation by reaction with either hexanoic anhydride or hexanoyl chloride leading to compound **7** and (ii) reduction of the resulting ketone using the Wolff–Kishner conditions or by using NaBH₄–AlCl₃ as reducing reagent. The resulting materials were characterized by ¹H and ¹³C NMR spectroscopy, mass spectrometry and elemental analysis as summarized in the Experimental Section.

SCHEME 1

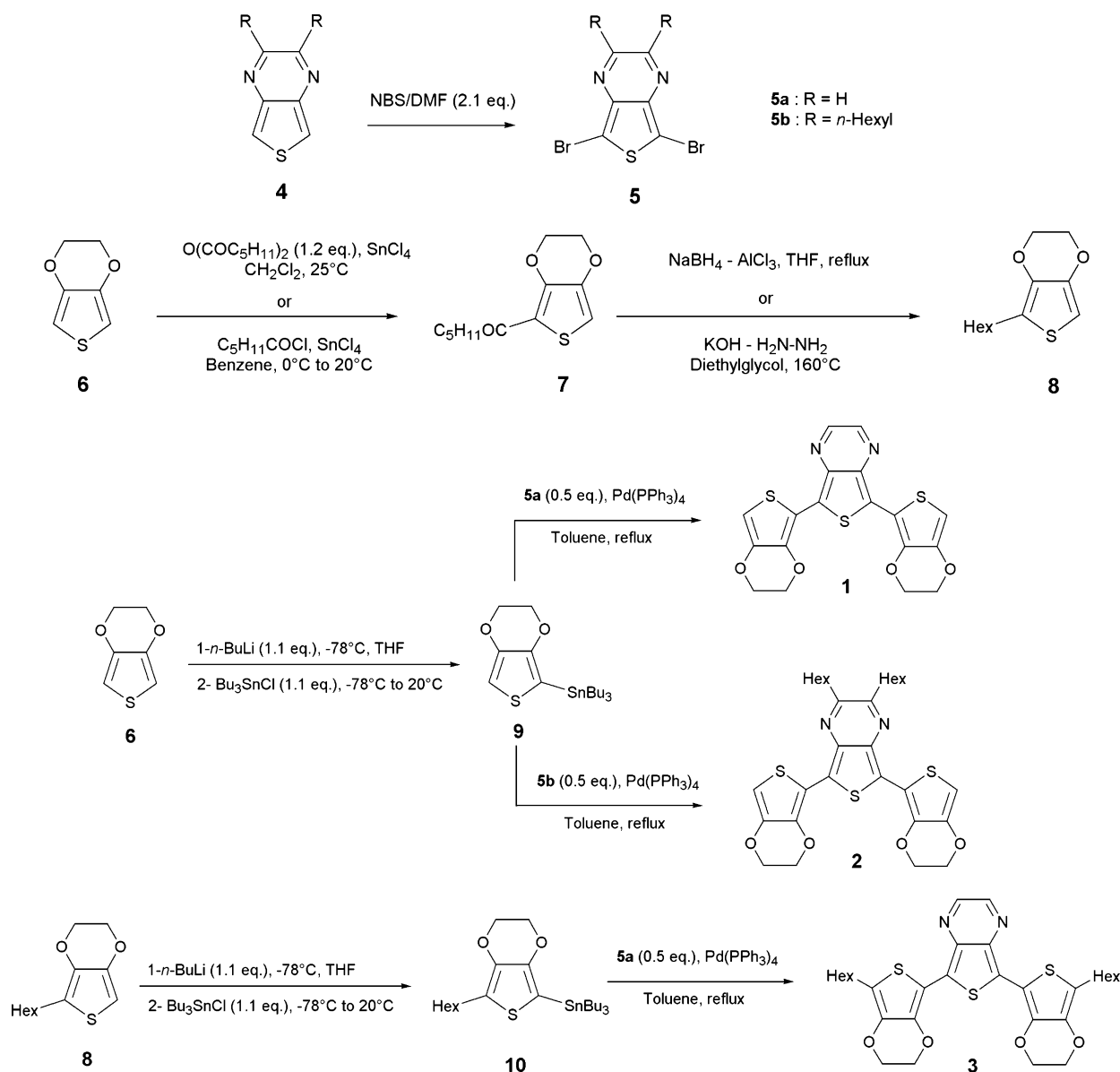


TABLE 1: UV-Vis Absorption Maxima (λ_{max}) of **1, **2**, and **3** in Dichloromethane Solution**

compound	CH ₂ Cl ₂ ^a
1	310, 344, 358, 375, 578
2	316, 339, 354, 372, 535
3	315, 354, 371, 390, 613

^a λ_{max} values in nm.

Table 1 lists the UV-vis absorption maxima (λ_{max}) of **1–3** in CH₂Cl₂ solution, whereas Figure 2 shows the UV-vis spectra of the three compounds. The materials display similar UV-vis features with two sharp absorptions around 315 and 350 nm (the latter showing a well-resolved fine structure with three distinct maxima) and a third broad band extending from around 450 to 700–750 nm. Thus, the optical data reveal that these π -conjugated mixed trimers are characterized by a small HOMO–LUMO separation, particularly in the case of **3**. The broad shape of these lowest energy bands seems to indicate the charge transfer character of their associated electronic promotions that could consist of an intramolecular excitation from the end-capping EDOT donor rings to the central electron-withdrawing thieno[3,4-*b*]pyrazine unit. The next sections are

especially devoted to establish precise structural-spectroscopic relationships governing these optical properties.

Comparison of the optical data for terthiophene (λ_{max} of the π – π^* transition at 350 nm) and trimers **1–3** shows that the combined effects of replacement of the median thiophene by thieno[3,4-*b*]pyrazine and the introduction of electron-releasing ethylenedioxy β -substituents and α, α' -hexyl end-caps produce a ca. 180–260 nm redshift of λ_{max} associated to the lowest-energy absorption, and hence a narrowing of the HOMO–LUMO gap.

The UV-vis spectra of the α -linked oligothiophenes are known to present a broad and structureless absorption band around 350–420 nm, due to the π – π^* transition, which reflects the conformational disorder upon solution of the π -conjugated thienyl units. The spectra of **1–3** exhibit a well-resolved fine structure, with the three distinct maxima of the vis absorption band centered at 350 nm being equally spaced by 1300–1350 cm^{–1} which is consistent with the coupling to the electronic structure of a $\nu(\text{C}=\text{C})$ stretching mode of the heteroaromatic moieties. The observation of vibronic transitions in solution is indicative of a strong rigidification of the π -conjugated backbone. This self-rigidification process results from the develop-

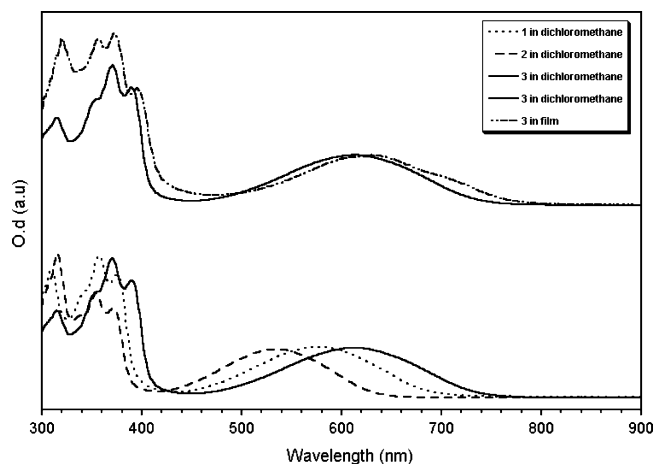


Figure 2. UV-vis absorption spectra of 1–3.

TABLE 2: Comparison between the CV Data for Compounds 1–3 and Those of Terthiophene

compound	E_{pa} (V)	E_{pr} (V)	$\Delta E = E_{pa} - E_{pr}$ (V)
1 ^a	0.58	−1.27	1.85
2 ^a	0.53	−1.58	2.11
3 ^a	0.53	−1.36	1.89
3T ^b	1.10	−2.00	3.10

^a Solution of compound (1 mM) in *n*-Bu₄NPF₆/CH₂Cl₂ 0.1 M, scan rate 100 mV s^{−1}, Pt working and counter electrodes, Ag/AgCl reference.

^b Reference 19.

ment of intramolecular closed-shell interactions between heteroatoms of the EDOT and thienopyrazine moieties as will be outlined in the sections referred to the crystalline structures and to the theoretical optimized geometries.^{18a,b,f} As can be seen in Figure 2, the UV-vis spectrum of a thin solid film of 3 on glass grown by high-vacuum sublimation is slightly blue-shifted by 20 nm compared to that obtained for dichloromethane solution. This shift is associated with solid-state interactions between the neighbor molecules what is confirmed by the X-ray data regarding the presence of close couples of molecules forming dimer species in the solid phase. However, the fact that the spectra obtained in solution or in solid state remain nearly superposable is in sharp contrast with the behavior observed for α,ω -dihexyloligothiophenes where the close-packed organization results in the formation of a crystalline film and hence in a splitting of the single excited state leading to a significant blue shift of the band observed in solution).^{18c–e}

B. Electrochemical Properties. Table 2 compares the cyclic voltammetric (CV) data for compounds 1–3 with those reported in the literature for terthiophene.¹⁹ Figure 3 shows the CV of 3 as a prototypical case. Each of the three mixed trimers 1–3 exhibit an irreversible oxidation wave at anodic peak potentials (E_{pa}) in the range of 0.53–0.58 V/Ag/AgCl corresponding to the formation of the radical cation. The one-electron oxidation processes occurred significantly lower than in the case of 3T at 1.10 V, what manifests a predominant effect of the terminal rich electron EDOT groups which favorably counterbalance the inclusion of an electron withdrawing thienopyrazine group. Compared to unsubstituted compound 1, the introduction of two electron releasing hexyl chains in 2 or 3 leads to a negative shift of E_{pa} (−50 mV). The irreversibility of the oxidation wave of 1 and 2 stems from the subsequent polymerization process which takes place at the electrode due to the occurrence of free α terminal positions. In fact, Zotti et al. have recently prepared compound 1 and successfully electro-polymerized it to a new low-optical gap (1.3 eV) polymer. A very interesting feature of

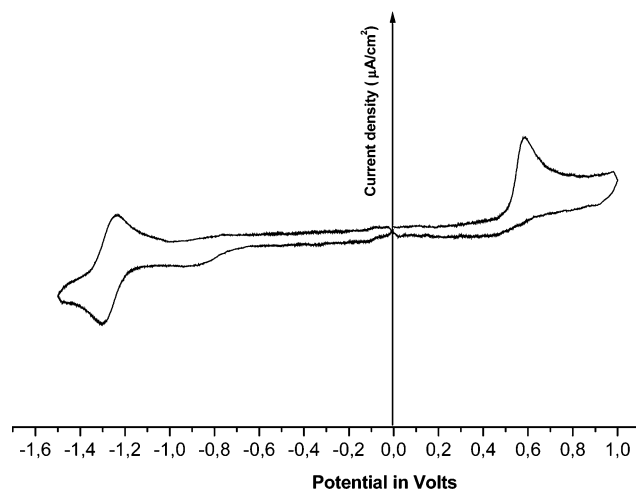


Figure 3. Cyclic voltammogram of 3 (0.053 mol L^{−1} in 0.1 mol L^{−1} Bu₄NPF₆/CH₂Cl₂, scan rate 100 mV s^{−1}).

this polymer material is that it displays the maximum of the absorption band in the near-IR region (950 nm), which can result of interest, for example, in solar cells.²⁰ In the case of our molecule 2, with hexyl chains on the pyrazine, the corresponding polymers exhibit a lower band gap (close to 1 eV) which is probably consistent with a longer polymer due to an enhanced solubility (see Figure S1, S2, and S3). On the other hand, although electropolymerization is prevented by the substitution of all α and β positions of thiophene rings, the existence of an irreversible oxidation wave in compound 3 is a puzzling finding. The electrochemical irreversibility for this oxidation is in stark contrast with the stability of the radical cation generated by chemical oxidation with FeCl₃, as checked by the maintenance of its chemically obtained UV-vis spectrum within a few hours in dichloromethane. If the cationic material reacts with the counterions of the electrolyte, or forms a film on the electrode by aggregation processes helped by the high propensity to π -dimerize, or if the electron-transfer kinetic is slow, then the CV scan will not be reversible. Similar irreversible processes have been already outlined by Cao et al.²¹ and by Turbiez et al.¹⁷ in oligothiophenes containing EDOT units.

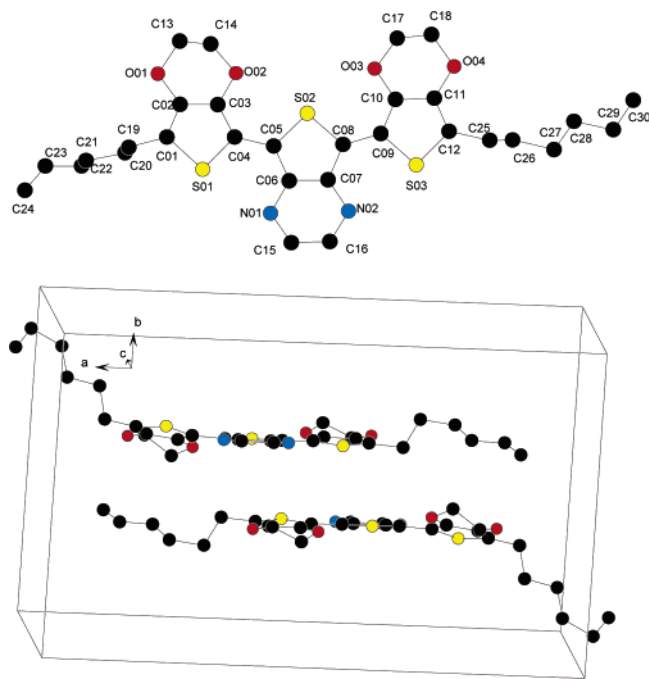
Table 3 show the natural population analysis (NPA) charge distribution in the cases of the radical cation and anion obtained at the B3LYP (closed shell systems) or UB3LYP/6-31G** (open shell systems) level of theory. Tables S1, S2, and S3 show the relevant geometrical parameters and atomic charges calculated for the cations and anions of 1 and 3. Unexpectedly for the cationic species, the injected charge is homogeneously distributed over the whole π -conjugated backbone so that even the central thienopyrazine ring of 3^{•+} bears $\approx 30\%$ of the net charge of the positively charged species. The accumulation of a partial positive charge in the pyrazine moiety could exalt the reactivity character of its nitrogens (−0.413 *e* for N4 of 3 in Figure 1 and +0.009 *e* in 3^{•+}) perhaps allowing further reactions at the basis of its irreversibility. The analysis of the 3 \rightarrow 3^{•+} optimized geometries also reveals the releasing effect of the rich electron outermost EDOT groups toward the central part since, upon one electron extraction, the C=C/C–C relaxation (quinoidization) following the generation of the charge defect is larger in the central unit.

On the other hand, compounds 1–3 can be reduced to the radical anion at various reduction peak potentials E_{pr} . Compared to 1 ($E_{pr} = -1.27$ V/Ag/AgCl), the introduction of hexyl chains in 2 and 3 produces a negative shift of the value of E_{pr} (−310 and −90 mV, respectively) in agreement with the positive

TABLE 3: Net NPA Charges (in e) in Excess or Defect (i.e., for the Radical Anion and Radical Cation, Respectively) over the Donor and Acceptor Units of **1 and **3**, as Deduced from the Comparison between the Theoretical Charge Distributions of the Neutral and Doped Species**

	1 ⁺	3 ⁺	1 ⁻	3 ⁻
thieno[3,4- <i>b</i>]pyrazine	+0.276 + 2 (+0.026) ^a	+0.255 + 2 (+0.024) ^a	-0.500 + 2 (-0.027) ^a	-0.486 + 2 (-0.026) ^a
each EDOT donor unit	+0.314 + (+0.022) ^b	+0.300	-0.199 + (-0.023) ^b	-0.196
each hexyl side chain		+0.050		-0.035

^a NPA atomic charge on each of the two hydrogens linked to the fused pyrazine ring. ^b NPA atomic charge on the hydrogen linked to the end α -position of the EDOT ring.

**Figure 4.** Front-view and solid-state packing views of **3**. Molecules have been omitted for clarity.

inductive effect of the alkyl groups. However, this effect is more pronounced in the case of **2** where the hexyl groups are directly connected on the thienopyrazine acceptor moiety likely due to phenomenon of hyperconjugation of the hexyl \leftrightarrow pyrazine groups in the case of the negatively charged species. Interestingly, whereas the reduction wave is irreversible for compounds **1** and **2**, that of **3** becomes reversible as shown in Figure 3 what accounts for the electroactivity blocking of these α terminal positions. After one-electron reduction, the greatest geometrical distortions take place for the innermost C–S bonds close to the fused pyrazine ring whose aromaticity gaining is the driving force for the electron injection process.

The three mixed trimers **1–3** exhibit smaller electrochemical gap values ($\Delta E = E_{\text{pa}} - E_{\text{pr}}$) than **3T** as the combined result of (i) the increase in electron affinity induced by the replacement of the central thienyl unit by a thienopyrazine moiety (which shifts the reduction peak potential, E_{pr} , to less energetic values) and (ii) the positive inductive effects of the ethylenedioxy and hexyl substituents (which lower the oxidation potentials). On the other hand, the ≈ 0.6 V decrease in E_{pa} and the 0.4–0.6 V positive shift of E_{pr} , indicated by the comparison of the cyclic voltammetry data of **1–3** and **3T**, show that the gap reduction in the three mixed trimers is due to the raising of the HOMO and lowering of the LUMO levels.

C. Crystallographic Structures, Optimized Geometries and Electronic Spectra. The crystal structure of compound **3** has been resolved and is shown in Figure 4. Long dark blue needles were obtained by slow liquid–liquid diffusion between a chloroform solution of **3** and methanol. X-ray diffraction

analysis revealed that the thiophene rings have an all-anti disposition and that dihedral angles between each thiophene rings only slightly deviated from planarity. Thus although one bithiophenic segment constituted by one EDOT and the central thienopyrazine ring formed a quasicoplanar system, the dihedral angle between the second external EDOT ring and the central thienopyrazine ring reached a relatively small deviation of 16°. Regarding the alkyl chains, that connected to the more planar bithiophene segment is roughly extended in the long axis of the molecule, whereas the other one is tilted 45° away from the mean plane of the molecule. These results show that in solid state the molecule exhibits a conformation of low symmetry (absence of the C_2 axis through the thienopyrazine ring). The examination of the crystal packing shows the presence of dimers of **3** along the b axis. The two molecules of the dimer adopt a head to tail arrangement and are staggered from one another leading to a partial overlap involving a thienopyrazine-EDOT segment. The distance between the two molecules inside the dimer has been calculated to 3.65(1) Å. However, there are negligible interactions between each dimer.

Assuming the already noted low molecular symmetry, the geometries of **1–3** were optimized, at the DFT//B3LYP/6-31G** level, without imposing any constraint. The all-anti coplanar arrangement of the three constituting rings is predicted as the lowest-energy structure in the gas-phase for the three compounds, with the hexyl substituents pointing out at the same side of the molecular plane by an angle of 35–45°. Geometrical features predicted by DFT model chemistry for these narrow-HOMO–LUMO gap mixed trimers as isolated entities in the vacuum are in excellent agreement with the close intramolecular distances observed in the crystal of **3**. Thus, there exist quite short inter-ring contacts between (a) the central sulfur atom and the oxygen atoms of the EDOT rings: 2.95–2.98 Å observed in the solid and 2.90 Å predicted by theory (the sum of their corresponding van der Waals radii is 3.25 Å) and (b) the thienopyrazine nitrogens and the sulfur atoms of the outermost EDOT: 2.98–3.01 Å as measured by X-ray diffraction or ≈ 3.00 Å as deduced from B3LYP/6-31G** model chemistry (the sum of their corresponding van der Waals radii is 3.35 Å). These attractive interactions between heteroatoms of successive α -linked units are closely related with the low values of dihedral angles between the thienyl rings as has been also observed for some related narrow-HOMO–LUMO gap mixed co-oligomers (for which steric hindrance to intramolecular rotation was almost negligible or absent).^{9b,18,a,b,f,22} Generally, strong intermolecular interactions, also based on short heteroatom contacts, help to improve the solid-state structural order and to enhance the charge transport between adjacent molecules.

As for **1**, the all-anti conformation is predicted to be 15.34 kcal/mol more stable than the all-syn one, which results to be the highest-energy structure due, among other factors, to the strong steric interaction between the pyrazine fused ring and the two 3,4-ethylenedioxy side chains. On the other hand, the $\phi_1 = \phi_2 = 90^\circ$ perpendicular arrangement (i.e., the molecular conformation less favorable to the π conjugation) is predicted

TABLE 4: Selected DFT//B3LYP/6-31G Skeletal Bond Lengths (in Å) for the Neutral Forms of 1–3**

bond	1	2	3	3 (X-ray) ^a
S ₁ –C ₂	1.752	1.753	1.753	1.712–1.740
C ₂ –C ₃	1.400	1.400	1.401	1.375–1.391
C ₃ –C ₇	1.442	1.434	1.443	1.429
C ₃ –N ₄	1.363	1.360	1.362	1.360–1.365
N ₄ –C ₅	1.314	1.317	1.314	1.316–1.296
C ₅ –C ₆	1.433	1.458	1.432	1.415
C ₂ –C ₈	1.434	1.434	1.433	1.473–1.438
C ₈ –S ₁₂	1.766	1.766	1.767	1.732–1.737
C ₈ –C ₉	1.385	1.385	1.385	1.350–1.355
C ₉ –C ₁₀	1.418	1.418	1.416	1.409–1.414
C ₁₀ –C ₁₁	1.367	1.366	1.370	1.350–1.347
C ₁₁ –S ₁₂	1.739	1.740	1.752	1.757–1.708
C ₉ –O ₁₃	1.359	1.360	1.360	1.380–1.370
O ₁₃ –C ₁₄	1.431	1.430	1.431	1.445–1.418
C ₁₄ –C ₁₅	1.573	1.569	1.558	1.490–1.446
C ₁₅ –O ₁₆	1.428	1.429	1.428	1.432–1.424
O ₁₆ –C ₁₀	1.361	1.361	1.366	1.372–1.367

^a Different values for the same bond in the unit cell.

to be 12.32 kcal/mol higher in energy than the all-anti one. These energy values can be compared with those previously obtained, at the same level of theory, for a related thieno[3,4-*b*]pyrazine moiety endowed by two thienyl rings.²¹ For the later compound, the lowest-energy all-anti conformer is only 1.22 kcal/mol more stable than the all-syn one (since the steric hindrance to intramolecular rotation is rather small, contrary to what happens for **1**), and the potential barrier to the highest-energy $\phi_1 = \phi_2 = 90^\circ$ arrangement amounted to 9.87 kcal/mol (value which can be attributed to the loss of both π conjugation and short inter-ring contacts). Thus, the attachment of 3,4-ethylenedioxy groups to the thienyl rings (i) increases the number of inter-ring contacts between heteroatoms of adjacent rings, (ii) modifies the π -conjugational properties of the mixed trimers due to their electron-releasing effect, and (iii) increases the steric hindrance during the rotation of the successive D/A units of the π -conjugated chain.

Table 4 summarizes the DFT//B3LYP/6-31G** optimized values for the main skeletal bond lengths of **1–3** in neutral state together with X-ray diffraction experimental values. The general matching between the theory and experiments is very satisfactory since the root-mean-square deviation between the experimental and theoretical bond lengths is of around 0.03 Å and its pearson correlation parameter is very close to 1 (0.998). This comparison reveals the good validity of our calculations since it is well-known in the literature that the DFT methodology tends to somewhat overestimate π conjugation, which, among other molecular parameters, translates in under/overestimating the C–C/C=C bond distances involved in the conjugated path.²³ The three molecules display a geometry quite similar to each other, and only subtle differences in bond lengths are noticed in the vicinity of the alkyl side groups. The major variations take place for **2** due to the steric hindrance between the two hexyl chains, so that the C₅–C₆ bond is found to lengthen by 0.025 Å with respect to the other two compounds. In all of the cases, the C₁₀–C₁₁ distance is the shortest (≈ 1.366 Å) among all of the CC bonds constituting the π -conjugated backbone of the system. We also notice that the DFT//B3LYP/6-31G** optimized values for the C₈–C₉ and C₉–C₁₀ bond lengths (i.e., 1.385 and 1.418 Å, respectively) are the same as those previously computed for two parent trimers bearing two end thienyl donor units covalently attached to either a central thienothiadiazole or a thienopyrazine acceptor moiety,²¹ but somewhat different from those previously found at the same level of theory for the outer rings of an α -linked terthiophene

with the two β positions of the central ring substituted by butyl side-chains (i.e., 1.380 and 1.423 Å).²⁴ These geometrical data suggest a certain increase of the overall π -conjugation in going from the homogeneous oligothiophenes to this type of mixed co-oligomers. The optimized length for the inter-ring C₂–C₈ bond of **1–3** (1.434 Å) also gives support to this conclusion, since in the three cases it is shorter by around 0.02 Å than in the aforementioned α -linked terthiophene (referred to as **3T** in Table 1 of ref 23).

The geometrical differences between **1–3**, on one hand, and the **3T** (terthiophene) taken as a reference, on the other hand, further extend to the innermost thienyl ring. In this regard, we also observe that the C₂–C₃ bond (1.400 Å) is longer than its counterpart in **3T** (1.385 Å). A feasible explanation for its lengthening could be a partial loss of π -electron density over the central thienyl unit due to the electron-withdrawing ability of the fused pyrazine ring, which however is expected to affect very little the C₂–S₁ and C₃–C₇ bonds in view that their B3LYP/6-31G** lengths are quite similar for the three narrow-HOMO–LUMO gap trimers (i.e., 1.752 and 1.442 Å, respectively, for **1**) and **3T** (1.751 and 1.441 Å).

The degree of bond length alternation (BLA), calculated as the difference between average lengths of the C–C and C=C bonds of the π -conjugated path, amounts to +0.045 Å for **1–3**, a value similar to that derived from the DFT//B3LYP/6-31G** optimization of 3',4'-dibutyl-5,5''-dinitro-2,2':5',2''-terthiophene (i.e., an electron-deficient π -conjugated system termed as NO₂T₃NO₂ in ref 24), whose π -conjugated spine structure evolves from the typical aromatic-like pattern of **3T** (with a BLA value of +0.063 Å) to a partially quinonoid-like pattern for which the BLA parameter significantly lowers. The quinoidization of the system is mainly induced by the attachment of a pyrazine ring to the thienyl central unit. This can be seen comparing the BLA values of compound **1** and 5,7-dithien-2-ylthieno[3,4-*b*]pyrazine (**TPT**), +0.045 and +0.043, respectively.^{21b} Similar BLA values to those of **1–3**, of $\approx +0.045$ Å, were also computed for some asymmetrically end-capped terthiophene having a pronounced push–pull character, such as 3',4'-dibutyl-5-nitro-5''-phenyl-2,2':5',2''-terthiophene and 3',4'-dibutyl-5-nitro-5''-bromo-2,2':5',2''-terthiophene.²⁴

Useful information can be gathered from the overall sum of all of the atomic charges on each ring (Tables S1, S2, and S3). The net charges on the donor EDOT rings and the central thieno[3,4-*b*]pyrazine acceptor moiety amount to +0.044 *e* and –0.088 *e* for **1**, +0.029 *e* and –0.059 *e* for **2**, and +0.052 *e* and –0.103 *e* for **3**. This theoretical electrostatic picture agrees with the UV–vis data and also suggests that, among the three chromophores, the highest ICT takes place for **3** and the lowest for **2**. Thus, the attachment of the hexyl side chains to the end α positions of the EDOT donor rings enhances the electron transfer to the central acceptor moiety, but their direct attachment to the fused pyrazine ring serves to partially reduce its electron affinity, due to the well-known positive inductive effects by the alkyl groups.

To investigate the nature of the electronic transitions that give rise to the UV–Vis absorption bands observed experimentally, the lowest-energy electronic excited states of **1–3** were calculated at the B3LYP/6-31G** level using the TDDFT approach on their optimized molecular geometries. Theoretical calculations predict the appearance of three strong electronic transitions in the UV–Vis region (see Table S4). The bands measured, in CH₂Cl₂ solution, at 2.15 eV (**1**), 2.32 eV (**2**), and 2.02 eV (**3**) are due to the excitation to the first singlet excited electronic state, which is computed at 1.95 eV for **1** (with a oscillator

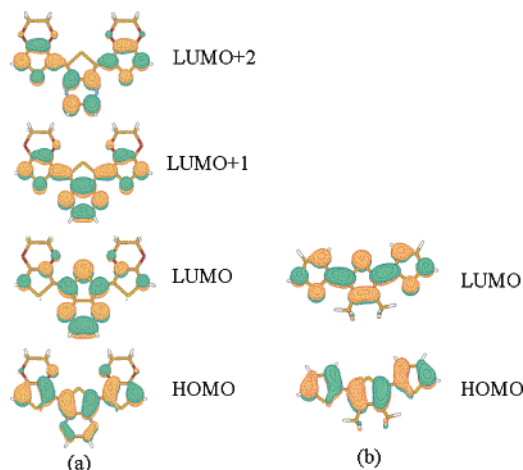


Figure 5. Electronic density contours ($0.03 e/\text{bohr}^3$) calculated at the B3LYP/6-31G** level for the HOMO, LUMO, LUMO+1 and LUMO+2 molecular orbitals of (a) **1** and for the HOMO and LUMO of (b) the model **3T** terthiophene.

strength, f , of 0.22), at 2.02 eV for **2** ($f = 0.22$) and at 1.86 eV for **3** ($f = 0.30$). This vertical transition is mainly described by a one-electron excitation from the highest occupied molecular orbital (HOMO) to the lowest unoccupied molecular orbital (LUMO). Although TDDFT model chemistry slightly underestimates by around 0.2 eV the experimental energies for the π - π^* transition, it however nicely accounts for the observed peak positions in passing from one chromophore to another.

The topologies of the frontier molecular orbitals involved in the main electronic absorptions of the compounds are sketched in Figure 5. For the three systems, the HOMO is of π nature and is delocalized over the whole π backbone (including a contribution by the fused pyrazine ring and by the innermost oxygens of both 3,4-ethylenedioxy- side chains). On the other hand, the LUMO is mainly located on the central electron-withdrawing moiety, contrary to what is usually found in α -linked oligothiophenes for which both HOMO and LUMO spread over the whole π -conjugated path.²³ Consequently, the HOMO \rightarrow LUMO transition implies certain electron density transfer from the aromatic-like donor EDOT rings to the more quinoid-like acceptor thienopyrazine unit and consequently the electronic features at 578 nm for **1**, 535 nm for **2**, and 613 nm for **3** correspond to D \rightarrow A \leftarrow D charge-transfer bands. Moreover, the HOMO and LUMO topologies show certain overlap, which is a prerequisite which leads this intramolecular charge transfer to arise important changes of the molecular hyperpolarizabilities and as a consequence to be of interest in non linear optics features.

One could in principle think that lowering of energy gap is mainly a consequence of the large stabilization of the LUMO, due to the strong electron-acceptor ability of the central *o*-quinoid ring. It has already been shown that, upon the attachment of electron-withdrawing groups at the end α positions of linear π -conjugated chains, the relative energies of the HOMO and LUMO move toward lower values with respect to the unsubstituted system, affecting the LUMO more than the HOMO and thus lowering the energy gap.^{23,23} However, DFT calculations for **1–3** reveal that relative to **3T** the insertion of an *o*-quinoid thieno[3,4-*b*]pyrazine electron-acceptor moiety between two donor EDOT rings stabilizes the LUMO but destabilizes the HOMO in a similar extent, thus causing a large reduction of the energy gap (Figure 6). This theoretically predicted absolute energy increasing of the HOMO level is the largest for **3** in agreement with its lowest oxidation potential,

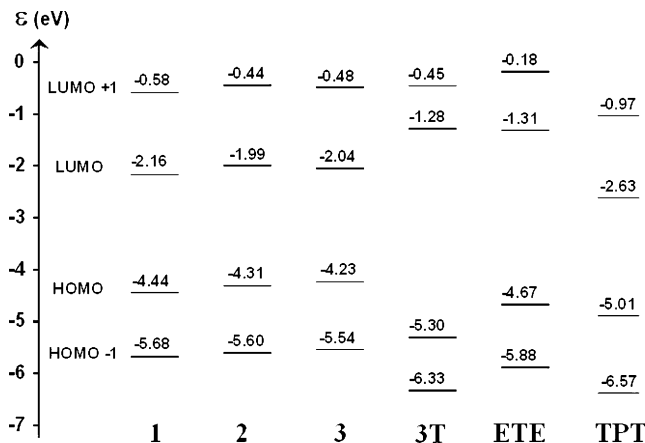


Figure 6. B3LYP/6-31G** one-electron energies (ϵ_i) diagram around the frontier molecular orbitals of **1–3** and of the models **3T**, **ETE**, and **TPT** terthiophenes taken as references.

furthermore the largest energy HOMO changes occur on **3T** \rightarrow **3** as observed experimentally in the oxidation potentials. Figure 6 shows detailed data of the absolute energy of the frontier orbitals for some intermediate cases between **3T** and **3**, 2,5-bis(2-(3,4-ethylenedioxy)thienyl)-thiophene (**ETE**) is included for comparison purposes. It is deduced that inclusion of EDO/pyrazine groups pushes up/down the HOMO/LUMO energies in agreement with their electron donor/acceptor character.

Calculations predict that the strong visible bands of **1** (3.31 eV), **2** (3.33 eV), and **3** (3.18 eV) arise from the HOMO \rightarrow LUMO+1 excitation, with the topologies of these MO being quite similar to those of the HOMO and LUMO involved in the characteristic π - π^* absorption of the homogeneous α -linked oligothiophenes (see for instance Figure 4 of ref 23), the only difference being a partial contribution by the fused pyrazine ring to the LUMO+1. As can be seen in Figure 6, the LUMO+1 of **1–3** are destabilized by ≈ 0.7 – 0.8 eV with respect to the LUMO of **3T**. However, the destabilization of the HOMO of **1–3** by ≈ 0.8 – 1.0 eV with respect to the HOMO in **3T** makes the HOMO \rightarrow LUMO+1 (**1–3**) and HOMO \rightarrow LUMO (**3T**) electronic transitions to have similar excitation energies. Thus, the strong vis absorption of these trimers at ≈ 380 nm is to be correlated with the π - π^* transition of the nonpolar α -linked oligothiophenes ≈ 350 nm.

The absorptions experimentally measured at 4.00 eV (**1**), 3.92 eV (**2**), and 3.94 eV (**3**) must be correlated to the transitions calculated for **1** at 4.37 eV ($f = 0.25$), for **2** at 4.16 eV ($f = 0.43$), and for **3** at 4.34 eV ($f = 0.19$). In the three cases, the electronic transition can be mainly described as the HOMO-5 \rightarrow LUMO excitation. Both MO are mainly located on the central electron-acceptor moiety, and thus the optical absorption bands of these molecules at ≈ 310 nm arise from an electronic transition of the *o*-quinoid thieno[3,4-*b*]pyrazine unit.

D. Vibrational Spectra. Figure 7 shows the infrared and Raman spectra of **2**. Let us restrict our discussion to the more relevant spectroscopic observations of general validity for this class of molecular materials. Usually, the unsubstituted (i.e., the nonpolar π -conjugated systems) display IR and Raman spectra which are complementary, in the sense that what is strong in the IR is weak in the Raman and vice versa.^{11–13} When the end α,ω positions of this oligomeric chain are attached to a donor and an acceptor group (push–pull chromophore with ICT), several vibrational normal modes become strongly active both in the IR and Raman spectra.^{12,17,25} In addition, the relative intensities of the infrared bands appearing for push–pull systems in the 1600–1000 cm^{-1} spectral region (namely, those associ-

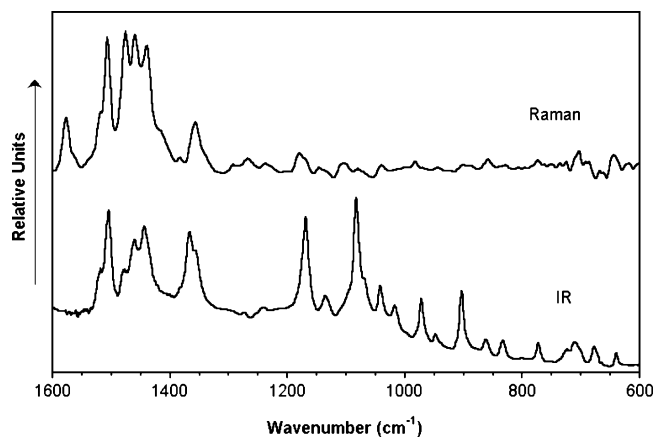


Figure 7. Comparison, over the 1600–600 cm^{-1} spectral region, between the FT-IR spectrum of **2** in the form of pressed KBr pellet and its FT-Raman spectrum as a pure solid sample.

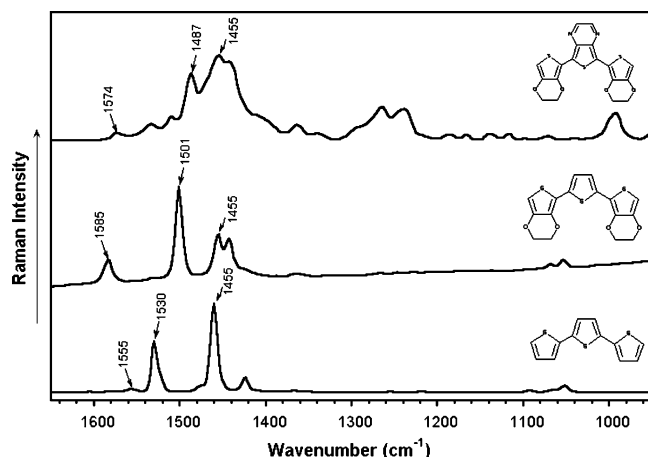


Figure 8. Comparison between the experimental FT-Raman spectra of (a) **3T** and (b) **3T** substituted its two outer rings with EDO groups and (c) **1**.

ated to skeletal vibrations of the π -conjugated backbone) are comparatively very much stronger than those recorded for the nonpolar oligothiophenes (for which the strongest IR absorptions are by far those appearing ≈ 800 and/or 670 cm^{-1} due to the out-of-plane $\gamma(\text{CH})$ deformations). We see that the situation is halfway for **2**, since its IR and Raman spectra show a great resemblance in the 1600–1300 cm^{-1} spectral region, whereas many other IR bands are recorded with a strong intensity below 1200 cm^{-1} although they lack a counterpart in the Raman scattering spectrum. This is a nice experimental evidence of the theoretically predicted existence of a polarized $(\text{D})^{\delta} + -(\text{A})^{\delta} -$ alternating structure (the B3LYP/6-31G** dipole moments amount to 5.84 D for **1**, 4.49 D for **2**, and 5.78 D for **3**; being between the 0.29 D value calculated for the nonpolar **3T** model of ref 23 and, by example, that of 11.4 D for the polarized push–pull system termed as **2b** in ref 25).

Raman spectroscopy allows us to compare the changes in the molecular/electronic structure upon successive substitution of **3T** with EDO and pyrazine groups; thus, Figure 8 compares the Raman spectra of **3T**, a **3T** with its two terminal rings substituted at β with EDO groups, and the Raman spectrum of **1**. The first observation is the increment of the band number on going from **3T** to **1** due to the appearance of different chemical frameworks for the thiophene rings; however, it is possible to establish relevant spectroscopic correlations emerging from electronic or structural effects. The band at 1555 cm^{-1} in **3T** is due to a C=C stretching mode located exclusively at the

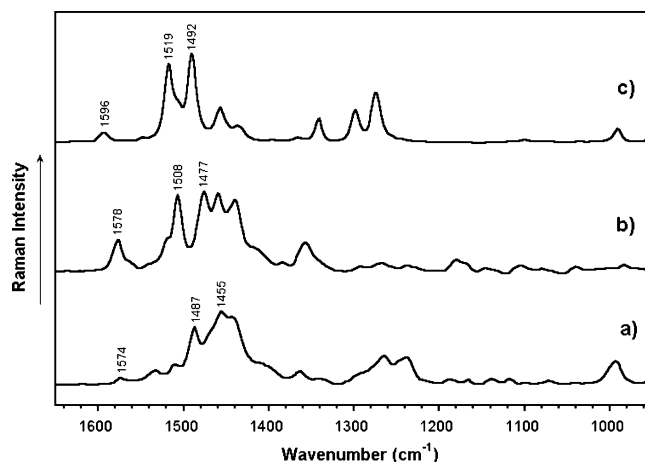


Figure 9. Comparison between the experimental FT-Raman spectra of (a) **1**, (b) **2**, and (c) **3** in solid state.

end thiophene rings which upshifts to 1585 cm^{-1} upon EDO substitution as a consequence of the strengthening of the C=C bonds induced by the oxygen positive inductive effect, but only to 1574 cm^{-1} in **1**, thus revealing certain weakening of the outermost EDOT C=C bonds upon charge transfer toward the central thienopyrazine moiety. The lines at 1530/1460 cm^{-1} in **3T** arise however from C=C stretching modes of the terminal/inner rings strongly coupled with the central/terminal thienyl C=C bonds motions. Given the collective character of these two skeletal vibrations their wavenumber values can be related with the theoretical BLA parameter which accounts for the efficiency of the π -electron conjugation in terms of bond lengths. Hence, these 1530/1460 cm^{-1} lines in **3T** evolve to 1487/1455 cm^{-1} in **1** in agreement with the $+0.063 \text{ \AA} \rightarrow +0.045 \text{ \AA}$ change of the BLA on **3T** \rightarrow **1**. This observation constitutes therefore a spectroscopic fingerprint of the increment in π -electron conjugation, or quinoidization, in **1** regarding **3T** which is halfway in the case of the EDO derivative of **3T** with Raman lines at 1501/1455 cm^{-1} . For this last case, the structural relaxation of the C=C/C–C conjugated path relative to that of **3T** might be a consequence of the favored scenario in a richer electron system and to the appearance of through space O \rightarrow S interactions which facilitate the rigidification and coplanarization of the whole system as seen by the analysis of the X-ray and theoretical data.

Figure 9 compares the solid-state Raman spectra of the three trimers under study. Their Raman spectra display a more complex spectral pattern than the usual homogeneous oligothiophenes. As aforementioned, the main Raman features appear above 1300 cm^{-1} , all of them being related to stretching vibrations of the C=C/C–C conjugated backbone (see Figures S4 and S5 in the Supporting Information regarding experimental/theoretical spectra comparison and vibrational eigenvectors). DFT quantum-chemical calculations allow us to correlate the wavenumbers of a given normal mode along the **1** \rightarrow **2** \rightarrow **3** series of compounds. The most outstanding values for the purpose of our study are the following: 1574 \rightarrow 1578 \rightarrow 1596 cm^{-1} , 1487 \rightarrow 1508 \rightarrow 1519 cm^{-1} , and 1455 \rightarrow 1477 \rightarrow 1492 cm^{-1} . The three vibrations are mainly due to C=C stretchings of the thienyl units, so that their peak positions can be used as markers of the structural changes induced by the attachment of the hexyl side chains at different positions of the conjugated rings. We see that upon hexylation the three modes experience a wavenumber upshift with respect to **1**, with it being significantly larger in the case of **3**. This spectroscopic observation can be interpreted in terms of the inductive positive effect (+I)

by part of the alkyl groups which translate into a strengthening of the conjugated C=C bonds. It follows that both **2** and **3** are electron-rich systems than **1**. As for **2**, the +I effect of the alkyl chains partially mitigates the electron withdrawing effect of the pro-aromatic fused pyrazine group over the central thiophene ring, thus resulting in a slightly more aromatic character of the π -conjugated backbone (namely, Raman scatterings at higher wavenumbers) in **2** than in **1**. The electron releasing effect of the two hexyl chains is even more pronounced when directly attached to the two end α positions of the outer thiophene rings, giving rise to the most electron rich system among the three chemicals. Thus, the Raman fingerprint of these mixed trimers are nicely in accordance with the lowest anodic electrochemical values for **3**. The whole effect is that the aromatic/quinoid character of the C=C/C-C conjugated path is subtly tuned by the positive inductive effect of the hexyl chains and increases following the **1** \rightarrow **2** \rightarrow **3** order in agreement with the upshift of the Raman scatterings associated to the C=C/C-C stretching modes.

III. Summary and Conclusions

In summary, we have reported on the synthesis and a careful and extended spectroscopic study of three novel narrow-HOMO-LUMO gap heterocyclic mixed trimers containing a *o*-quinoid electron-acceptor thienopyrazine central moiety endowed by two donor EDOT units and with different patterns of hexyl functionalization. The affectation of the terthiophene structure upon EDO, pyrazine, and hexyl substitution has been treated in detail with spectroscopic and theoretical arguments. The X-ray diffraction data and the DFT/B3LYP/6-31G** molecular geometry optimizations performed for all of the compounds have revealed the occurrence of short intramolecular contacts between heteroatoms of adjacent rings. The analysis of the structure of the π -conjugated backbone of each neutral molecule is consistent with a partial quinoid-like pattern for the three trimers regarding its terthiophene homologue and an increasing aromaticity tuned by the positive inductive effect of the hexyl chains. The quinoidization of the electronic structure in these trimers is a consequence of the appearance of a **D**(EDOT) \rightarrow **A**(PyT) \leftarrow **D**(EDOT) intramolecular charge transfer which further polarizes the structure. The effectiveness of this ICT mechanism is sensitive to the hexyl positions through a subtle interplay of +I \leftrightarrow quinoid \leftrightarrow aromatic balances. The same chemical concepts modulating the electronic structure of these compounds apply for their electrochemical behavior. The three mixed trimers exhibit a smaller electrochemical gap ($\Delta E = E_{\text{pa}} - E_{\text{pr}}$) than terthiophene as the combined result of (i) the increase in electron affinity upon the replacement of the central thienyl ring by a thienopyrazine moiety (which shifts the reduction peak potential, E_{pr} , to less energetic values) and (ii) the positive inductive effects from the ethylenedioxy and hexyl side chains which render a richer π -electron system (thus lowering the oxidation potential).

From a material point of view, this work provides useful information on a few building blocks monomers for electropolymers. Given their relative low HOMO-LUMO energy gap, these trimers promise to be good candidates for obtaining polymer of very low energy gap. In fact **poly-1** has been successfully obtained by others²⁰ showing interesting near-IR absorption properties what might be of great interest in, for example, for photon-to-electrical conversion applications. Presently these systems themselves have already been proved as materials combining very interesting optical and electrochemical

properties. In this sense our future objective will deal with further physicochemical studies of their homologue polymers.

IV. Experimental and Theoretical Details

¹H NMR and ¹³C NMR spectra were recorded on a Bruker Avance DRX 500 spectrometer operating at 500.13 and 125.7 MHz, respectively; δ are given in ppm (relative to TMS) and coupling constants (*J*) in Hz. UV-vis-NIR absorption spectra were recorded on a Perkin-Elmer Lambda 19 spectrometer. Melting points were obtained from a Reichert-Jung Thermovar hot-stage microscope apparatus and are uncorrected. Elemental analysis was performed by the Service Central d'Analyses of CNRS (Vernaison, France). Column chromatography purifications were carried out on a MERCK silica gel Si 60 (40–63 μm).

Mass spectrometry analyses were performed on a JMS-700 (JEOL LTD, Akishima, Tokyo, Japan) double focusing mass spectrometer with reversed geometry, equipped with a pneumatically assisted electrospray ionization (ESI) source. MALDI-TOF spectra were recorded on a MALDI-TOF-MS BIFLEX III Bruker Daltonics spectrometer. Nitrogen was used as the nebulizer gas. The sample was diluted in a chloroform solution or in CHCl₃/CH₃CN (70/30) mixture and introduced into the ESI interface via a syringe pump (PHD 2000 infusion; Harvard Apparatus, Holliston, MA) at a 40 $\mu\text{L min}^{-1}$ flow rate. A 5 kV acceleration voltage was applied and elemental composition of ions were checked by high-resolution measurements using an electric-field scan with a mixture of PGEs as internal standard with nominal molecular weights centered around 1000.

Crystallographic Data for Compound 3. C₃₀H₃₆N₂O₄S₃, *M* = 584.79, Monoclinic, space group *P*2₁/*c*, *a* = 24.115(2) Å, *b* = 14.863(1) Å, *c* = 8.4076(7) Å, β = 88.86(1)°, *V* = 3012.9(4) Å³, *Z* = 4, *D*_c = 1.289 g/cm³, μ = 0.283 mm⁻¹. *R*₁[*I* > 2 σ (*I*)] = 0.0578, *wR*₂ = 0.107, *S* = 0.752 for 1861 observed reflections and 352 parameters.

Data collection was carried out at 293K on a STOE-IPDS diffractometer using graphite-monochromated Mo K α radiation (λ = 0.71073 Å). The structure was solved by direct methods (SIR92) and refined by full-matrix least-squares on *F*² with SHELXL97. Absorption effects were empirically corrected by multiscan method. All non-hydrogen atoms were refined with anisotropic displacement parameters. Hydrogens atoms were treated with a riding model.³⁴

Fourier transform infrared absorption (FT-IR) spectra were recorded on a Bruker Equinox 55 spectrometer. Compounds were ground to a powder and pressed in KBr pellets. FT-IR spectra, with a spectral resolution of 2 cm⁻¹, were collected and 50 scans were averaged. Interference from atmospheric water vapor was minimized by purging the instrument with dry argon before starting the data collection. FT-Raman scattering spectra were collected on a Bruker FRA106/S apparatus and a Nd:YAG laser source (λ_{exc} = 1064 nm), in a backscattering configuration. The operating power for the exciting laser radiation was kept to 100 mW in all the experiments. Samples were analyzed as pure solids in sealed capillaries and dilute CH₂Cl₂ and DMSO solutions (supplied by Aldrich with analytical grade). Typically, 1000 scans with 2 cm⁻¹ spectral resolution were averaged to optimize the signal-to-noise ratio.

Cyclic voltammetry was performed in CH₃CN or CH₂Cl₂ solutions (with HPLC grade). Tetrabutylammonium hexafluorophosphate (0.1 M as supporting electrolyte) or metal perchlorate were purchased from Fluka (Fluka puriss) and used as received, without further purification. Solutions were deaerated by N₂ bubbling prior to each measurement, which was also run

under a continuous nitrogen gas flow. Electrochemical experiments were performed in a one-compartment cell equipped with a platinum working microelectrode ($\varnothing = 1$ mm) and a platinum wire counter electrode. An Ag/AgCl electrode checked against ferrocene/ferricinium couple (Fc/Fc^+) before and after each experiment was used as reference. Electrochemical experiments were carried out with a PAR 273 potentiostat with positive feedback compensation.

Density functional theory (DFT) calculations were carried out by means of the Gaussian 98 program²⁶ running on an SGI Origin 2000 supercomputer. We used the Becke's three-parameter exchange functional combined with the LYP correlation functional (B3LYP).²⁷ It has already been shown that the B3LYP functional yields similar geometries for medium-sized molecules as MP2 calculations do with the same basis sets.^{28,29} Moreover, the DFT force fields calculated using the B3LYP functional yield infrared spectra in very good agreement with experiments.^{30,31} We also made use of the standard 6-31G** basis set.³² Optimal geometries were determined on isolated entities. All geometrical parameters were allowed to vary independently apart from planarity of the rings. On the resulting ground-state optimized geometries, harmonic vibrational frequencies and infrared and Raman intensities were calculated analytically with the B3LYP functional.

We used the often-practiced adjustment of the theoretical force fields in which calculated harmonic vibrational frequencies are uniformly scaled down by a factor of 0.96 for the 6-31G** calculations, as recommended by Scott and Radom.³⁰ This scaling procedure is often accurate enough to disentangle serious experimental misassignments. All quoted vibrational frequencies reported along the paper are thus scaled values. The theoretical spectra were obtained by convoluting the scaled frequencies with Gaussian functions (10 cm^{-1} width at the half-height). The relative heights of the Gaussians were determined from the theoretical Raman scattering activities.

Vertical electronic excitation energies were computed by using the time-dependent DFT (TDDFT) approach.^{33,34} The twelve lowest-energy electronic excited states were at least computed for all of the molecules. The computational cost of TDDFT is roughly comparable to that of single-excitation theories based on an HF ground state, such as single-excitation configuration interactions (CIS). Numerical applications reported so far indicate that TDDFT formalism employing current exchange-correlation functionals performs significantly better than HF-based single excitation theories for the low-lying valence excited states of both closed-shell and open-shell molecules.^{35,36} TDDFT calculations were carried out using the B3LYP functional and the 6-31G** basis set on the previously optimized molecular geometries obtained at the same level of calculation.

Radical anions and radical cations were treated as open-shell systems and were computed using spin-unrestricted UB3LYP wave functions. The maximum value obtained for S^2 was 0.76, very close to the 0.75 theoretically expected for a doublet, showing that spin contamination is almost absent.

5,7-Dibromothieno[3,4-b]pyrazine (5a). Under a N_2 atmosphere and in the absence of light, a solution of *N*-bromosuccinimide (0.88 g, 4.94 mmol) in DMF (15 mL) was added over a period of 15 min to a solution of **4a** (0.32 g, 2.35 mmol) in DMF (30 mL) cooled to -25°C . The mixture was stirred for 2 h at -25°C and then allowed to warm to 20°C . The reaction mixture was poured into water (200 mL), and the mixture was extracted with CH_2Cl_2 (3×100 mL). The organic phases were washed with water (100 mL) and dried (MgSO_4), and the solvent

was removed under reduced pressure. The crude product was purified by column chromatography on silica gel (eluent: EtOAc) affording a dark solid which was dissolved in a mixture of solvents CHCl_3 /petroleum ether (6 mL/25 mL). The black precipitate was separated by filtration under suction and the filtrate solution was concentrated under vacuum leading to a yellow-brown powder (0.37 g, 48% yield). M.p. 205°C . ^1H NMR (CDCl_3) δ : 8.53 (s, 2H). ^{13}C NMR (CDCl_3) δ : 105.8, 140.6, 145.6. EI MS m/z (I%): 294 (M^+ , 100).

2,3-Dihexyl-5,7-dibromothieno [3,4-b]pyrazine (5b). Under a N_2 atmosphere and in the absence of light, a solution of *N*-bromosuccinimide (2.27 g, 12.78 mmol) in DMF (50 mL) was added over a period of 20 min to a solution of **4b** (1.85 g, 6.08 mmol) in DMF (110 mL) cooled to -25°C . The mixture was stirred for 2 h at -25°C and then allowed to warm to 20°C . The reaction mixture was poured into water (500 mL) and the mixture was extracted with CH_2Cl_2 (4×150 mL). The organic phases were washed with water (100 mL) and dried (MgSO_4), and the solvent was removed under reduced pressure. The crude product was purified by column chromatography on silica gel (eluent: CH_2Cl_2 /Petroleum ether 1:2) affording a green-dark solid (1.77 g, 63% yield). M.p. 64°C . ^1H NMR (CDCl_3) δ : 0.91 (t, 6H, $^3J = 7.0$ Hz); 1.32–1.39 (m, 8H); 1.43–1.49 (m, 4H); 1.76–1.83 (m, 4H); 2.90 (t, 4H, $^3J = 7.8$ Hz). ^{13}C NMR (CDCl_3) δ : 14.1, 22.6, 27.9, 29.2, 31.7, 35.3, 103.1, 139.3, 158.2.

2-Hexanoyl-3,4-ethylenedioxythiophene (7). *Method A.* Under a N_2 atmosphere, a solution of hexanoic anhydride 97% (9.83 g, 0.045 mol) in anhydrous CH_2Cl_2 (100 mL) was added to a solution of EDOT (5.12 g, 0.036 mol) in anhydrous CH_2Cl_2 (2 mL). A 1 M solution of SnCl_4 in CH_2Cl_2 (45 mL, 0.045 mol) was then added dropwise, and the reaction mixture was stirred for 24 h. The red-brownish mixture was poured into a mixture of ice (100 mL) and acetic acid (30 mL). After separation of the organic phase by decantation, the aqueous phase was extracted with CH_2Cl_2 (3×60 mL). The organic phases were gathered, washed with a 10% aqueous solution of NaOH until neutralization of AcOH, and dried (MgSO_4). After concentration to dryness, the residue was purified by chromatography on silica gel (eluent CH_2Cl_2) to give a white solid (2.41 g, 28% yield). *Method B.* Under a N_2 atmosphere, hexanoic chloride (0.98 mL, 7.04 mmol) was added to a solution of EDOT (1 g, 7.04 mmol) in anhydrous benzene (10 mL) cooled to 0°C . Anhydrous SnCl_4 (1.83 g, 7.02 mmol) was added dropwise, and the reaction mixture was then allowed to warm to 20°C and was further stirred for 1 h. A mixture of concentrated HCl (2 mL) and water (18 mL) was added to the red-brownish mixture which turned blue-green. The mixture was extracted with Et_2O (3×100 mL). The combined extracts were washed with water (3×75 mL), dried (Na_2SO_4), and evaporated in vacuo. After chromatography on silica gel (eluent: CH_2Cl_2), compound **7** was obtained as a beige solid (0.67 g, 40% yield). M.p. $89\text{--}90^\circ\text{C}$. ^1H NMR (CDCl_3) δ : 0.91 (t, 3H, $^3J = 7.0$ Hz); 1.33–1.38 (m, 4H); 1.70 (quint., 2H, $^3J = 7.4$ Hz); 2.84 (t, 2H, $^3J = 7.4$ Hz); 4.23–4.26 (m, 2H); 4.36–4.39 (m, 2H); 6.67 (s, 1H). IR (KBr) $\nu\text{ cm}^{-1}$: 1643 (C=O).

2-Hexyl-3,4-ethylenedioxythiophene (8). *Method A.* Under a N_2 atmosphere, a mixture of compound **7** (0.50 g, 2.08 mmol), NaBH_4 (0.40 g, 10.52 mmol), and anhydrous AlCl_3 (0.76 g, 5.71 mmol) in anhydrous THF (25 mL) was refluxed for 2.5 h and left under stirring overnight. The reaction mixture was cooled to 0°C , and water (20 mL) was added dropwise. After extraction with EtOAc (4×50 mL), the organic phases were dried (Na_2SO_4) and concentrated under reduced pressure.

Purification by chromatography on silica gel (eluent CH₂Cl₂/Petroleum ether 1:1) gave compound **8** as colorless oil (0.12 g, 25% yield). *Method B.* Under a N₂ atmosphere, a mixture of compound **7** (3 g, 12.5 mmol), KOH (2.8 g, 50 mmol), and hydrazine hydrate 80% (3 mL) in diethylglycol (70 mL) was heated to 160 °C for 20 min, after which time all starting material was consumed. The reaction mixture was cooled to 20 °C, and a 0.5 M aqueous solution of HCl was added (100 mL). After extraction with Et₂O (3 × 150 mL), the organic phase was washed with an aqueous saturated solution of NaCl (200 mL), dried (Na₂SO₄), and concentrated under reduced pressure. Purification by chromatography on silica gel (eluent CH₂Cl₂/Petroleum ether 1:1) gave compound **8** as a colorless oil (0.54 g, 19% yield). ¹H NMR (CDCl₃) δ: 0.90 (t, 3H, ³J = 6.5 Hz); 1.32–1.39 (m, 4H); 1.40 (m, 2H); 1.58 (quint., 2H, ³J = 7.6 Hz); 2.63 (t, 2H, ³J = 7.5 Hz); 4.17 (m, 4H); 6.11 (s, 1H). ¹³C NMR (CDCl₃) δ: 14.1, 22.6, 25.9, 28.8, 30.4, 31.5, 64.5, 64.7, 94.9, 118.4, 137.3, 141.4. EI MS *m/z* (I%): 226 (M⁺, 100).

5,7-Bis(3,4-ethylenedioxy-2-thienyl)thieno[3,4-b]pyrazine (1). Under a N₂ atmosphere, a mixture of 5,7-dibromothieno[3,4-b]pyrazine **5a** (13 mg, 0.044 mmol) and the stannyl derivative of EDOT **9** (60 mg, 0.139 mmol, 3 eq.) in the presence of Pd(PPh₃)₄ (5 mg, 0.004 mmol, 10% mol) in N₂ degassed toluene (15 mL) was refluxed for 3 h. The reaction mixture was cooled to 20 °C and concentrated to dryness. Addition of petroleum ether to the residue led to precipitation of a black powder and then the petroleum ether solution was separated by decantation. The resulting black powder was subjected a second time to the same treatment to remove the excess of compound **9**. The black powder was then purified by chromatography on silica gel (eluent: CH₂Cl₂) leading to a purple powder (1.5 mg, 8% yield). M.p. > 260 °C. ¹H NMR (CDCl₃) δ: 4.31–4.33 (m, 4H); 4.47–4.49 (m, 4H); 6.45 (s, 2H); 8.51 (s, 2H). MALDI-TOF MS (Dithranol) *m/z* (I%): 415.98.

2,3-Dihexyl-5,7-bis(3,4-ethylenedioxy-2-thienyl)thieno[3,4-b]pyrazine (2). Under a N₂ atmosphere, a mixture of 5,7-dibromothieno[3,4-b]pyrazine **5b** (1.25 g, 2.70 mmol) and the stannyl derivative of EDOT **9** (3.50 g, 8.11 mmol, 3 eq.) in the presence of Pd(PPh₃)₄ (0.31 g, 0.27 mmol, 10% mol.) in N₂ degassed toluene (100 mL) was refluxed for 16 h. The reaction mixture was cooled to 20 °C and concentrated to dryness. The residue was subjected to two successive purifications by chromatography on silica gel (eluent: CH₂Cl₂/Petroleum ether 1:1) affording a purple product (*R*_f = 0.52 in CH₂Cl₂/petroleum ether 1:1) which was then triturated in MeOH, filtered under suction, and washed successively with MeOH and pentane to give trimer **2** as a purple powder (0.59 g, 37% yield). A sample was recrystallized from a mixture of CH₃OH/EtOH to give purple needles. M.p. 129–132 °C (powder). ¹H NMR (CDCl₃) δ: 0.92 (t, 6H, ³J = 7.1 Hz); 1.35–1.42 (m, 8H); 1.49–1.55 (m, 4H); 1.98 (quint., 4H, ³J = 7.4 Hz); 2.91 (t, 4H, ³J = 7.4 Hz); 4.29–4.32 (m, 4H); 4.45–4.48 (m, 4H); 6.41 (s, 2H). ¹³C NMR (CDCl₃) δ: 14.1, 22.6, 26.7, 29.0, 31.8, 34.8, 65.3, 64.6, 100.2, 111.6, 121.3, 136.7, 137.5, 141.1, 155.0. EI MS *m/z* (I%): 584 (M⁺, 100), 487 (33), 292 (7). HRMS: calcd for C₃₀H₃₆N₂O₄S₃ 584.1837, found 584.1818. Anal. for C₃₀H₃₆N₂O₄S₃. Found (calcd.): C, 61.90 (61.62); H 6.29 (6.20); N, 4.70 (4.79); O, 11.59 (10.94); S, 15.81 (16.45).

5,7-Bis(3,4-ethylenedioxy-5-hexyl-2-thienyl)thieno[3,4-b]pyrazine (3). Under a N₂ atmosphere, a mixture of 5,7-dibromothieno[3,4-b]pyrazine **5a** (0.31 g, 1.05 mmol) and the stannyl derivative of 2-hexyl EDOT **10** (1.63 g, 3.16 mmol, 3

eq.) in the presence of Pd(PPh₃)₄ (0.12 g, 0.11 mmol, 10% mol.) in N₂ degassed toluene (50 mL) was refluxed for 24 h. The reaction mixture was cooled to 20 °C and concentrated to dryness. The residue was subjected to two successive purifications by chromatography on silica gel (using pure CH₂Cl₂ as the eluent for the first one and CH₂Cl₂/Petroleum ether/Et₃N 50:49:1 for the second one) affording a dark blue product which was then triturated in refluxing petroleum ether, filtered under suction, and washed with hot petroleum ether to give trimer **3** as a dark blue powder (86 mg, 14% yield). Long blue dark needles for X-ray analysis³⁷ were obtained by slow diffusion of a solution of **3** in CHCl₃ into MeOH. M.p. 242 °C (powder). ¹H NMR (CDCl₃) δ: 0.89 (t, 6H, ³J = 6.9 Hz); 1.29–1.32 (m, 8H); 1.36–1.40 (m, 4H); 1.67 (quint., 4H, ³J = 7.6 Hz); 2.70 (t, 4H, ³J = 7.7 Hz); 4.28–4.30 (m, 4H); 4.44–4.45 (m, 4H); 8.46 (s, 2H). ¹³C NMR (CDCl₃) δ: 14.1, 22.6, 26.1, 28.9, 30.4, 31.6, 64.6, 65.5, 107.0, 120.2, 122.8, 137.8, 138.2, 142.7. MALDI-TOF MS (Dithranol) *m/z* (I%): 584.01. Anal. for C₃₀H₃₆N₂O₄S₃. Found (calcd.): C, 61.64 (61.62); H 6.23 (6.20); N, 4.64 (4.79); O, 11.08 (10.94); S, 16.74 (16.45).

Acknowledgment. J.C., R.P.O., M.C.R.D., V.H., and J.T.L.N. acknowledge the Dirección General de Enseñanza Superior (DGES, MEC, Spain) for financial support to the investigation performed at the University of Málaga through Project BQU2003-03194. Part of the research was also supported by the Junta de Andalucía (Spain) under Grant FQM-0159. J.C. thanks the Ministerio de Ciencia y Tecnología (MCyT) of Spain for a “Ramón y Cajal” position of chemistry at the University of Málaga. M.C.R.D. and R.P.O. thank respectively the MEC and Junta de Andalucía for personal grants. P.B. and J.R. are indebted to France-Telecom for financial support and to the Service Commun d’Analyses Spectroscopiques d’Angers to the work at the University of Angers.

Supporting Information Available: Tables S1–S4 showing the theoretical bond lengths, charge distributions for the neutral and charged systems, the theoretical bond lengths, and TD-DFT assignments of the electronic absorption spectra. Figure S1 and S2 give the electrochemical properties of poly(**2**), and Figure S3 shows the electronic absorption spectra of poly(**2**) in the neutral and doped state. Figure S4 compares the theoretical and experimental Raman spectra of **2** and Figure S5 shows the vibrational eigenvectors associated with the most relevant lines of the spectrum of **2**. This material is available free of charge via the Internet at <http://pubs.acs.org>.

References and Notes

- (1) (a) Wudl, F.; Kobayashi, M.; Heeger, A. J. *J. Org. Chem.* **1984**, *49*, 3382. (b) Kobayashi, M.; Colaneri, M.; Boysel, M.; Wudl, F.; Heeger, A. J. *J. Chem. Phys.* **1985**, *82*, 5717.
- (2) (a) Kürti, J.; Surján, P. R.; Kertesz, M. *J. Am. Chem. Soc.* **1991**, *113*, 9865. (b) Karikomi, M.; Kitamura, C.; Tanaka, S.; Yamashita, Y. *J. Am. Chem. Soc.* **1995**, *117*, 6791.
- (3) Roncali, J. *Chem. Rev.* **1997**, *97*, 173.
- (4) (a) Sariciftci, N. S.; Smilowitz, L.; Heeger, A. J.; Wudl, F. *Science* **1992**, *258*, 1474. (b) Kraabel, B.; Hummelen, J. C.; Vacar, D.; Moses, D.; Sariciftci, N. S.; Heeger, A. J. *J. Chem. Phys.* **1996**, *104*, 4267.
- (5) Havinga, E. E.; ten Hoeve, W.; Wynberg, H. *Polym. Bull.* **1992**, *29*, 119.
- (6) Havinga, E. E.; ten Hoeve, W.; Wynberg, H. *Synth. Met.* **1993**, *55–57*, 299.
- (7) Meng, H.; Tucker, D.; Chaffins, S.; Chen, Y.; Helgeson, R.; Dunn, B.; Wudl, F. *Adv. Mater.* **2003**, *15*, 146.
- (8) Kitamura, C.; Tanaka, S.; Yamashita, Y. *Chem. Mater.* **1994**, *8*, 570.

- (9) (a) Akoudad, A.; Roncali, J. *Chem. Commun.* **1998**, 2081. (b) Perepichka, I.; Levillain, E. L.; Roncali, J. *J. Mater. Chem.* **2004**, *14*, 1679. (c) Raimundo, J. M.; Blanchard, P.; Brisset, H.; Roncali, J. *Chem. Commun.* **2000**, 939.
- (10) (a) Tanaka, S.; Yamashita, Y. *Synth. Met.* **1993**, *55–57*, 1251. (b) Hanack, M.; Schmid, U.; Röhrig, U.; Toussaint, J.-M.; Adant, C.; Brédas, J.-L. *Chem. Ber.* **1993**, *126*, 1487. (c) Ferraris, J. P.; Bravo, A.; Kim, W.; Hrnčir, D. C. *J. Chem. Soc., Chem. Commun.* **1994**, 991. (d) Kitamura, C.; Tanaka, S.; Yamashita, Y. *J. Chem. Soc., Chem. Commun.* **1994**, 1585. (e) Akoudad, A.; Roncali, J. *Chem. Commun.* **1998**, 2081.
- (11) Sakamoto, A.; Furukawa, Y.; Tasumi, M. *J. Phys. Chem.* **1994**, *98*, 4635.
- (12) (a) Yokonuma, N.; Furukawa, Y.; Tasumi, M.; Kuroda, M.; Nakayama, J. *Chem. Phys. Lett.* **1996**, *255*, 431. (b) Harada, I.; Furukawa, Y. *Vibrational Spectra and Structure*; Durig, J., Ed.; Elsevier: Amsterdam, 1991; Vol. 19, p 369.
- (13) (a) Hernández, V.; Casado, J.; Ramírez, F. J.; Zotti, G.; Hotta, S.; López Navarrete, J. T. *J. Chem. Phys.* **1996**, *104*, 9271. (b) Casado, J.; Hernández, V.; Hotta, S.; López Navarrete, J. T. *J. Chem. Phys.* **1998**, *109*, 10419. (c) Moreno Castro, C.; Ruiz Delgado, M. C.; Hernández, V.; Hotta, S.; Casado, J.; López Navarrete, J. T. *J. Chem. Phys.* **2002**, *116*, 10419. (d) Moreno Castro, C.; Ruiz Delgado, M. C.; Hernández, V.; Shirota, Y.; Casado, J.; López Navarrete, J. T. *J. Phys. Chem. B* **2002**, *106*, 7163.
- (14) (a) Casado, J.; Otero, T. F.; Hotta, S.; Hernández, V.; Ramírez, F. J.; López Navarrete, J. T. *Opt. Mater.* **1998**, *9*, 82. (b) Casado, J.; Hernández, V.; Hotta, S.; López Navarrete, J. T. *Adv. Mater.* **1998**, *10*, 1258. (c) Casado, J.; Miller, L. L.; Mann, K. R.; Pappenfus, T. M.; Kanemitsu, Y.; Ortí, E.; Viruela, P. M.; Pou-Amerigo, P.; Hernández, V.; López Navarrete, J. T. *J. Phys. Chem. B* **2002**, *106*, 3872. (d) Casado, J.; Miller, L. L.; Mann, K. R.; Pappenfus, T. M.; Hernández, V.; López Navarrete, J. T. *J. Phys. Chem. B* **2002**, *106*, 3597. (e) Casado, J.; Ruiz Delgado, M. C.; Shirota, Y.; Hernández, V.; López Navarrete, J. T. *J. Phys. Chem. B* **2003**, *107*, 2637.
- (15) Hernández, V.; Casado, J.; Effenberger, F.; López Navarrete, J. T. *J. Chem. Phys.* **2000**, *112*, 5105; González, M.; Segura, J. L.; Seoane, C.; Martín, N.; Garín, J.; Orduna, J.; Alcalá, R.; Villacampa, B.; Hernández, V.; López Navarrete, J. T. *J. Org. Chem.* **2001**, *66*, 8872.
- (16) (a) Zerbi, G.; Castiglioni, C.; Del Zoppo, M. *Electronic Materials: The Oligomer Approach*; Wiley-VCH: Weinheim, Germany, 1998; p 345. (b) Castiglioni, C.; Gussoni, M.; López Navarrete, J. T.; Zerbi, G. *Solid State Commun.* **1988**, *65*, 625. (c) López Navarrete, J. T.; Zerbi, G. *J. Chem. Phys.* **1991**, *94*, 957 and 965. (d) Hernández, V.; Castiglioni, C.; Del Zoppo, M.; Zerbi, G. *Phys. Rev. B* **1994**, *50*, 9815. (e) Agosti, E.; Rivola, M.; Hernández, V.; Del Zoppo, M.; Zerbi, G. *Synth. Met.* **1999**, *100*, 101. (f) Zerbi, G. *Handbook of Conducting Polymers*; Dekker: New York, 1998.
- (17) (a) Kenning, D. D.; Mitchell, K. A.; Calhoun, T. R.; Funfar, M. R.; Sattler, D. J.; Rasmussen, S. C. *J. Org. Chem.* **2002**, *67*, 9073. (b) Joussemle, B.; Blanchard, P.; Levillain, E.; de Bettignies, R.; Roncali, J. *Macromolecules* **2003**, *36*, 3020. (c) Turbiez, M.; Frère, P.; Roncali, J. *J. Org. Chem.* **2003**, *68*, 5357.
- (18) (a) Raimundo, J. M.; Blanchard, P.; Frère, P.; Mercier, N.; Ledoux-Rak, I.; Hierle, R.; Roncali, J. *Tetrahedron Lett.* **2001**, *42*, 1507. (b) Leriche, P.; Turbiez, M.; Monroche, V.; Blanchard, P.; Skabara, P. J.; Roncali, J. *Tetrahedron Lett.* **2003**, *44*, 649. (c) Yassar, A.; Horowitz, P.; Valat, P.; Wintgens, M.; Hmyene, M.; Deloffire, F.; Srivastava, P.; Lang, P.; Garnier, F. *J. Phys. Chem.* **1995**, *99*, 9155. (d) Dimitrakopoulos, C. D.; Malefrant, P. *Adv. Mater.* **2002**, *14*, 99. (e) de Bettignies, R.; Nicolas, Y.; Blanchard, P.; Levillain, E.; Nunzi, J.-M.; Roncali, J. *Adv. Mater.* **2003**, *15*, 1939. (f) Raimundo, J. M.; Blanchard, P.; Gallego-Planas, N.; Mercier, N.; Ledoux-Rak, I.; Hierle, R.; Roncali, J. *J. Org. Chem.* **2002**, *99*, 5341.
- (19) Jones, D.; Guerra, M.; Favaretto, L.; Modelli, A.; Fabrizio, M.; Distefano, G. *J. Phys. Chem.* **1990**, *94*, 5761.
- (20) Berlin, A.; Zotti, G.; Zecchin, S.; Schiavon, G.; Vercelli, B.; Zanelli, A. *Chem. Mater.* **2004**, *16*, 3667.
- (21) Cao, J.; Curtis, M. D. *Chem. Mater.* **2003**, *15*, 4424.
- (22) (a) Kitamura, C.; Tanaka, S.; Yamashita, Y. *Chem. Mater.* **1996**, *8*, 205. (b) Ruiz Delgado, M. C.; Hernández, V.; López Navarrete, J. T.; Tanaka, S.; Yamashita, Y. *J. Phys. Chem. B* **2004**, *108*, 2516.
- (23) (a) Hsu, C.-P.; Hirata, S.; Head-Gordon, M. *J. Phys. Chem. A* **2001**, *105*, 451. (b) Hirata, S.; Lee, T. J.; Head-Gordon, M. *J. Chem. Phys.* **1999**, *111*, 8904. (c) Heinze, H. H.; Görling, A.; Rösch, N. *J. Chem. Phys.* **2000**, *113*, 2088. (d) Grimme, S.; Parac, M. *ChemPhysChem* **2003**, *3*, 292. (e) Ehrendorfer, Ch.; Karpfen, A. *J. Phys. Chem.* **1994**, *98*, 7492. (f) Ehrendorfer, Ch.; Karpfen, A. *J. Phys. Chem.* **1995**, *99*, 5341. (g) Choi, C. H.; Kertesz, M.; Karpfen, A. *Chem. Phys. Lett.* **1997**, *276*, 266. (h) Yang, S.; Olshevskii, P.; Kertesz, M. *Synth. Met.* **2004**, *141*, 171.
- (24) Casado, J.; Pappenfus, T. M.; Miller, L. L.; Mann, K. R.; Ortí, E.; Viruela, P. M.; Pou-Amerigo, R.; Hernández, V.; López Navarrete, J. T. *J. Am. Chem. Soc.* **2003**, *125*, 2524.
- (25) Ruiz Delgado, M. C.; Hernández, V.; Casado, J.; López Navarrete, J. T.; Raimundo, J.-M.; Blanchard, P.; Roncali, J. *Chem. Eur. J.* **2003**, *9*, 3670.
- (26) Frisch, M. J.; Trucks, G. W.; Schlegel, H. B.; Scuseria, G. E.; Robb, M. A.; Cheeseman, J. R.; Zakrzewski, V. G.; Montgomery, J. A.; Stratman, R. E.; Burant, S.; Dapprich, J. M.; Millam, J. M.; Daniels, A. D.; Kudin, K. N.; Strain, M. C.; Farkas, O.; Tomasi, J.; Barone, V.; Cossi, M.; Cammi, R.; Mennucci, B.; Pomelli, C.; Adamo, C.; Clifford, S.; Ochterski, G.; Petersson, A.; Ayala, P. Y.; Cui, Q.; Morokuma, K.; Malick, D. K.; Rabuck, A. D.; Raghavachari, K.; Foresman, J. B.; Cioslowski, J.; Ortiz, J. V.; Stefanov, B. B.; Liu, G.; Liashenko, A.; Piskorz, I.; Komaromi, I.; Gomperts, R.; Martin, R. L.; Fox, D. J.; Keith, T.; Al-Laham, M. A.; Peng, C. Y.; Manayakkara, A.; González, C.; Challacombe, M.; Gill, P. M. W.; Johnson, B. G.; Chen, W.; Wong, M. W.; Andres, J. L.; Head-Gordon, M.; Replogle, E. S.; Pople, J. A. *Gaussian 98*, revision A.7; Gaussian, Inc.: Pittsburgh, PA, 1998.
- (27) Becke, A. D. *J. Chem. Phys.* **1993**, *98*, 1372.
- (28) Stephens, P. J.; Devlin, F. J.; Chabalowski, F. C. F.; Frisch, M. J. *J. Phys. Chem.* **1994**, *98*, 11623.
- (29) Novoa, J. J.; Sosa, C. *J. Phys. Chem.* **1995**, *99*, 15837.
- (30) Scott, A. P.; Radom, L. *J. Phys. Chem.* **1996**, *100*, 16502.
- (31) Rauhut, G.; Pulay, P. *J. Phys. Chem.* **1995**, *99*, 3093.
- (32) Francl, M. M.; Pietro, W. J.; Hehre, W. J.; Binkley, J. S.; Gordon, M. S.; Defrees, D. J.; Pople, J. A. *J. Chem. Phys.* **1982**, *77*, 3654.
- (33) (a) Runge, E.; Gross, E. K. U. *Phys. Rev. Lett.* **1984**, *52*, 997. (b) Gross, E. K. U.; Kohn, W. *Adv. Quantum Chem.* **1990**, *21*, 255. (c) Gross, E. K. U.; Dreizler, R. M., Eds.; Plenum Press: New York, 1995; pp 149.
- (34) Casida, M. E. *Recent Advances in Density Functional Methods, Part I*; Chong, D. P., Ed; World Scientific: Singapore, 1995; p 115.
- (35) Koch, W.; Holthausen, M. C. *A Chemist's Guide to Density Functional Theory*; Wiley-VCH: Weinheim, Germany, 2000.
- (36) Casado, J.; Miller, L. L.; Mann, K. R.; Pappenfus, T. M.; Kanemitsu, Y.; Ortí, E.; Viruela, P. M.; Pou-Amerigo, R.; Hernández, V.; López Navarrete, J. T. *J. Phys. Chem. B* **2002**, *106*, 3872.
- (37) Sheldrick, G. M. *SHELXL97 [Includes SHELXS97, SHELXL97, CIFTAB], Programs for Crystal Structure Analysis (Release 97–2)*, Göttingen, Germany, 1998.